Lab on a Chip
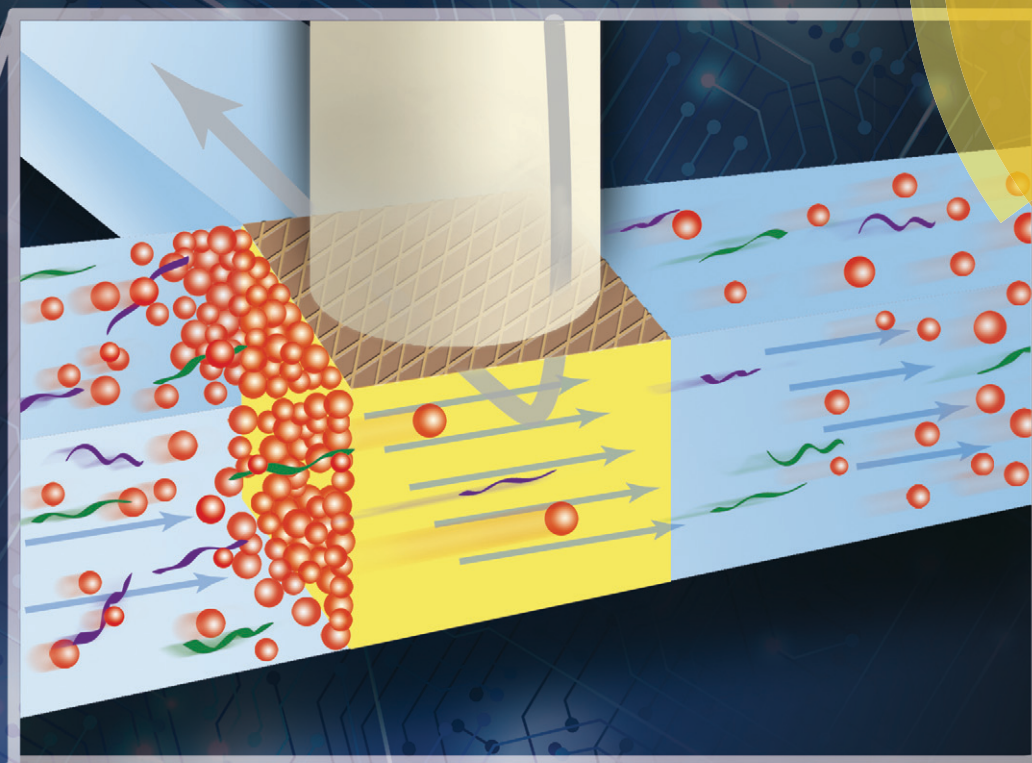
Miniaturisation for chemistry, physics, biology, materials science and bioengineering

www.rsc.org/loc

ROYAL SOCIETY
OF CHEMISTRY

PAPER
Hsueh-Chia Chang *et al.*
High-flux ionic diodes, ionic transistors and ionic amplifiers based on
external ion concentration polarization by an ion exchange membrane: a
new scalable ionic circuit platform

175 YEARS

Lab on a Chip

High-flux ionic diodes, ionic transistors and ionic amplifiers based on external ion concentration polarization by an ion exchange membrane: a new scalable ionic circuit platform†

Gongchen Sun, Satyajyoti Senapati and Hsueh-Chia Chang*

A microfluidic ion exchange membrane hybrid chip is fabricated using polymer-based, lithography-free methods to achieve ionic diode, transistor and amplifier functionalities with the same four-terminal design. The high ionic flux (>100 μA) feature of the chip can enable a scalable integrated ionic circuit platform for micro-total-analytical systems.

Introduction

Non-linear micro/nanofluidic circuit components like ionic diodes and ionic transistors may allow precise control of ion and biomolecule transport in integrated micro/nano total analytical systems for various wearable/implantable automated drug delivery, on-chip molecular analysis, point-of-care diagnostics and energy conversion applications.[1–3] Like semiconductor transistors and PN junction diodes that control electron/hole transport by alteration of their local densities,[4] ion-selective media, such as inorganic nanochannels,[5–7] asymmetric nanopores,[8] hydrated nanoporous dielectric layers,[9,10] and polymer-based ion-selective membranes or polyelectrolyte layers[11,12] can modulate ion concentrations in an electrolyte environment to realize similar circuit functionalities for ions and charged biomolecules. For example, an ion-selective silicon dioxide nanochannel coupled with electrostatic gating can form a nanofluidic transistor for switchable DNA transport;[6] a bipolar membrane junction can be operated as an ionic Zener diode to split water and establish local pH gradients for protein separation;[13,14] a permselective membrane can exhibit a nonlinear resistance shift when capturing charged biomolecules for ion current biosensing,[11,15] and can be easily linked with other microfluidic techniques such as on-chip surface acoustic wave lysis for rapid nucleic acid detection from raw samples directly.[16] If the aforementioned ionic circuit elements can be further synthesized into large-scale ionic circuits, massively multiplexed smart sensor arrays

can then be integrated with different molecular separation and concentration functionalities to analyze a large library of disease biomarkers with minimum analyte loss.[11,16] Spatial and temporal release of drugs using molecular delivery elements coupled to the detection platform can then be envisioned in future autonomous transdermal and implantable therapeutic devices.[17,18] Of course, soft matter-based ionic memory elements will also require similar large-scale integration.[19,20]

There is, however, a major hurdle in integrating ionic circuits. Almost all ionic diodes and ionic transistors to date realize specific non-linear circuit functions by modulating ion concentrations inside ion-selective media, such as within nanochannels or assembled charged polyelectrolytes.[6,7,12] Because of the nanoscale Debye-length dimensions of channels/pores within ion-selective media, these devices can only deliver low ion fluxes (less than a few hundred nanoamperes) and do not permit significant fluid flows due to their large hydrodynamic resistance. Furthermore, ionic transistors that allow bistable switches (on/off) do not amplify the ion current. Due to these low-flux limitations, current ionic circuit devices do not provide sufficient power to sustain a long-range ion current flux and feedback necessary for integrated circuits. Low ionic fluxes and high fluidic resistance also limit the possibility of using these ionic circuit elements to facilitate smart free-flow electrophoretic chips for high-throughput biomolecule separation,[21] and smart energy convertors for reverse electrodialysis platforms or electrical-to-mechanical energy conversion.[3,22–24]

Here, we report a simple but versatile method to build high-flux ionic diodes and ionic transistors in a high ionic strength environment by controlling the external rather than the internal ion concentration of an ion-selective membrane with two competing electric fields. An anion exchange membrane (AEM), coupling a control/input fluidic channel and an

Center for Microfluidics and Medical Diagnostics, Department of Chemical and Biomolecular Engineering, University of Notre Dame, Notre Dame, 46556, IN, USA. E-mail: hchang@nd.edu; Fax: + 574 631 8366; Tel: + 574 631 5697

output fluidic channel, can change the conductance of the output channel in a proper field direction across the AEM. With four electrode terminals for the two channels to control the two competing electric fields so that a particular electric field direction is imposed at the AEM, high-flux ionic diodes and transistors can then result from the same two-channel microfluidic anion exchange membrane hybrid design such that the output channel current can be rectified, switched on/off or amplified. Both the ionic diode and transistor can deliver an ion current of up to hundreds of microamperes with a few milliwatts of output power. No gel or polyelectrolyte component is used in the fluidic channel that delivers the output ion current; hence, the device is compatible with any free-flow operation that can rapidly refresh aqueous fluids and analytes for high-throughput operation. The fabrication of the device does not require elaborate semiconductor fabrication steps, such as lithography and etching, and can hence be massively produced for simple and low-cost manufacturing.

Results and discussion

Fig. 1 presents the device configuration and the key mechanism. As shown in Fig. 1a, the fluidic channel between the "G" and the "B" terminal is the control/input fluidic channel,
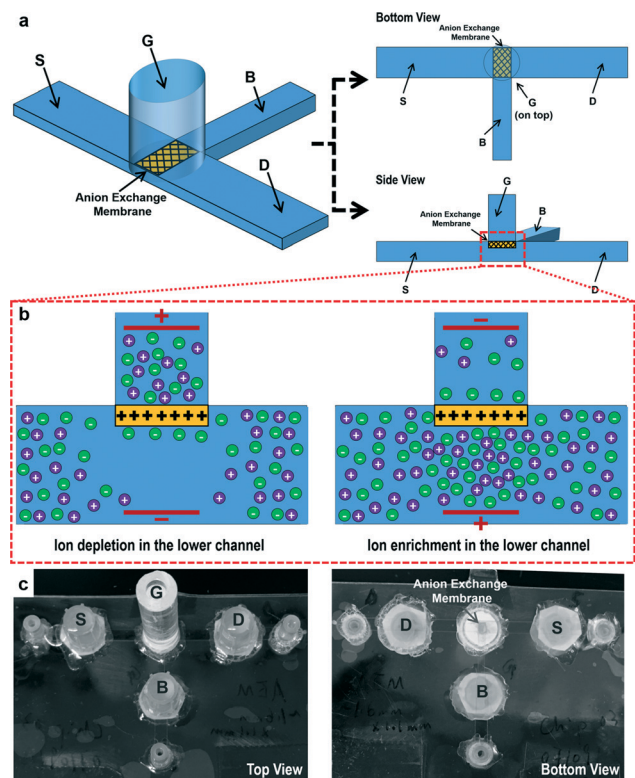

Fig. 1 (a) Schematics of the microfluidic anion exchange membrane (AEM) hybrid device by coupling the "G-B" control fluidic channel and the "D-S" output fluidic channel with an AEM. (b) Schematics of the external ion concentration polarization of the AEM. (c) The actual image of the device.

with the "G" terminal in the reservoir above the channel plane. A commercially-available AEM (see the ESI†) is sealed and placed below the "G" terminal reservoir, connecting the "G" terminal reservoir to the microfluidic channel in such a way that any movement of ions from or to the "G" terminal under an electric field always occurs through the AEM. The output channel is designed to be between the "D" and the "S" terminal. This output fluidic channel intersects with the control/input fluidic channel in a perpendicular manner right underneath the AEM. The ionic strength and conductance at this intersection region regulates the ion current through the output fluidic channel. The geometrical relationships between the AEM and the microfluidic plane and between the "G-B" control fluidic channel and the "D-S" output fluidic channel are important to maintain the stability of the designed ionic circuit platform, which will be discussed later. Since only negatively charged ions can pass through the AEM, the applied electric field across the membrane can induce external ion concentration polarization, with either depletion or enrichment on one side depending on the field direction.[11] As illustrated in Fig. 1b, when the electrical potential in the "G" terminal reservoir is sufficiently higher than the potential under the membrane (in the channel), a depletion zone with low ionic strength can be established in the intersection region, with the electric field directed away from the AEM. The depletion "*blocks*" the ion current through the output fluidic channel. Conversely, when reversing the polarities of the electrical potential in the "G" terminal reservoir and the one under the membrane, such that the electric field in the intersection region is towards the AEM, an enrichment zone with high ionic strength emerges in the intersection region, thus "enhancing" the ion current through the output fluidic channel. Ideally, both anion exchange membranes (AEM) and cation exchange membranes (CEM) can be used to build such an ionic circuit platform. Only the applied electric field direction needs to be reversed to create similar ion depletion/enrichment conditions at the intersection region if a CEM is used. In our chip design, an AEM is chosen since AEMs have shown the capability to be used in various biosensing applications, especially nucleic acid detection, based on our previous studies.[11,15,16] An ionic circuit platform built by AEMs can hence allow for direct integration with multiple AEM-based biosensing technologies.

Fig. 1c shows the actual device. The microfluidic channels are built by three layers of polycarbonate sheets. The "D-S" output fluidic channel is 28 mm in length, 2 mm in width and 250 μm in height. The "G-B" control fluidic channel is 12 mm in length, 1 mm in width and 250 μm in height. These two channels create a 1 mm × 2 mm intersection in the channel plane, above which a 1.1 mm × 1.6 mm AEM connects the "G" terminal reservoir and the intersection region. The AEM is embedded in a circular polyurethane resin pellet and fabricated using a specific molding protocol.[25] A PMMA tubing glued to the resin pellet serves as the "G" terminal reservoir. The reservoirs for the three electrical terminals "D", "S" and "B" are cut pipette tips and are separated

from the channels by filter papers and a layer of 1% agarose gel to prevent possible bubble entry into the channels. All the electrical signals are transmitted into the microfluidic channel using platinum electrodes. Tygon tubings are glued to the end of each channel as fluidic inlets and outlets. To demonstrate that the device is robust under high ionic strength conditions, we use 0.1× phosphate-buffered saline (PBS) solution as the electrolyte in all the experiments. 100 µM Rhodamine 6G dye is added into the 0.1× PBS solution in the channel as a fluorescence indicator to demonstrate the ion depletion and enrichment process at the intersection region. The positively charged Rhodamine 6G molecule is selected as it is not permeable to the AEM and also does not non-specifically adsorb to the AEM, which helps maintain the integrity of the membrane. All the fluorescence images are taken from the bottom of the device. The material information, chip fabrication and all the electrical measurements are described in detail in the ESI.†

Whether the device works as an ionic diode or an ionic transistor depends on the electrical operation method, *i.e.* the potential relationship at the four terminals and the net field at the AEM due to the competition between the two resulting electric fields. The ionic diode is configured as
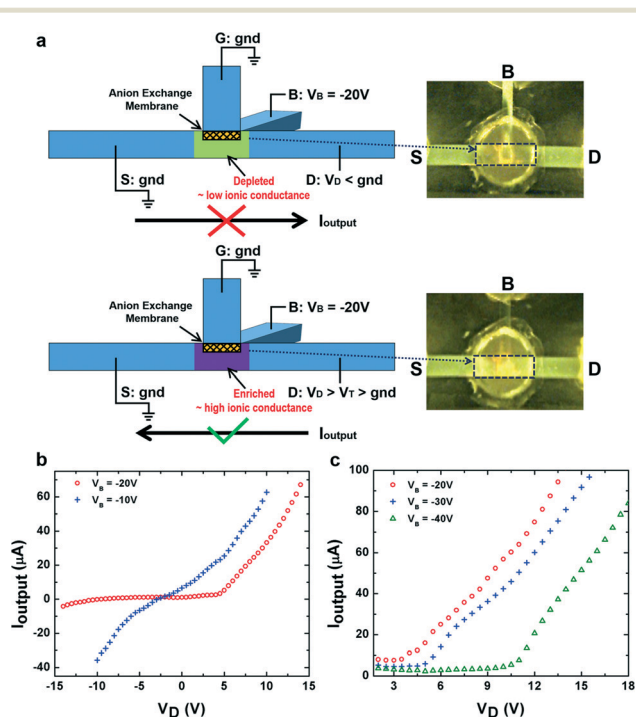

Fig. 2 (a) Schematics of the electrical operation method and the rectification mechanism of the ionic diode. The fluorescence images show the ion depletion in the reversed output current direction (the upper panel) and the ion enrichment in the forward output current direction (the lower panel) in the intersection region. (b) The output I–V characteristics under two different V_B values show that the output current rectification can be achieved when V_B = −20 V. V_D is swept from −14 V to 14 V for V_B = −20 V, while from −10 V to 10 V for V_B = −10 V. (c) The output I–V characteristics on the conductive side under three different V_B values show the modulation of the "on" threshold voltage of the ionic diode. V_D is swept from 0 V in each measurement.

shown schematically in Fig. 2a. The "G" terminal and the "S" terminal are co-grounded as a reference potential of the device. The applied voltage at the "B" terminal, V_B, works as a control voltage to regulate the ion concentration at the intersection region. The key design of the ionic diode involves lowering the ion conductance at the output fluidic channel by ion depletion with the output current in one direction and increasing the ion conductance by weakening the ion depletion when the output current is in the opposite direction. Here, the ion depletion is generated by setting the control voltage V_B as a negative potential (due to the AEM used) to ensure an ion depletion zone under the membrane through the "G-B" control fluidic channel, with the field direction away from the AEM.

As illustrated in the upper panel of Fig. 2a, when V_B is set as −20 V and the applied output potential V_D at the "D" terminal is lower than the potential at the "S" terminal – gnd, as well as the "G" terminal, the ion concentration at the intersection region remains depleted. The ion depletion after applying a negative V_D is indicated by the low fluorescence intensity at the intersection region (in the highlighted frame) shown in the upper panel of Fig. 2a. The output fluidic channel therefore maintains a low ionic conductance so that a very small output ion current I_{output} can flow in the direction from the "S" terminal to the "D" terminal. However, as illustrated in the lower panel of Fig. 2a, when the polarity of V_D is reversed and is above a sufficiently high positive value, the ion depletion at the intersection region is weakened. The positive V_D reverses the field direction as it renders the local potential under the AEM higher than gnd – the potential at the "G" terminal, even though V_B still keeps the same negative value. This field direction enriches the ion concentration at the intersection region and dramatically increases the current I_{output} in the output fluidic channel in the direction from the "D" terminal to the "S" terminal. The transformation from ion depletion to ion enrichment at the intersection region can be seen from the much higher fluorescence intensity at the intersection (in the highlighted frame) in the lower panel of Fig. 2a. It is worth noting that the fluorescence intensity in the rest of the "G-B" control fluidic channel remains low because the ion enrichment is confined to the intersection region that turns the output fluidic channel on.

We sweep V_D from −14 V to 14 V while keeping V_B at −20 V to demonstrate ion current rectification of the ionic diode, as shown by the hollow circular data points in Fig. 2b. The output ion current I_{output} is close to zero in the reversed direction (from terminal "S" to "D"), while it increases rapidly in the forward direction (from terminal "D" to "S") when the positive V_D exceeds a threshold value (∼ 4 V). I_{output} shows a 176 rectification factor at ±10 V. In contrast, I_{output} measurement with a V_D sweep from −10 V to 10 V at V_B = −10 V does not show appreciable rectification, as shown by the cross data points in Fig. 2b, indicating that the potential difference between the "G" terminal and the "B" terminal is not enough to fully generate the ion depletion zone at the intersection region. Thus, the "D-S" output fluidic channel maintains a high

and similar ionic conductance for both directions of I_{output}. Unlike most nanofluidic diodes or polyelectrolyte diodes which produce ion current rectification by ion enrichment and depletion within nanochannels or polyelectrolytes, our ionic diode employs external ion depletion and enrichment at the intersection region adjacent to the ion-selective nanoporous membrane. Hence, this ionic diode allows a much higher ion current flowing through the "D-S" microchannel when enrichment occurs at the intersection region (up to tens to hundreds of microamperes). Other than offering a high flux with the microfluidic channel, the ion exchange capacity of the selected AEM is not affected by the electrolyte ion concentration, since the 1 nm pore size within the AEM provides a strongly overlapped Debye layer over a wide range of buffer ionic strengths (see the ESI†).[15] Hence, the external ion depletion can be established even at high ion concentrations, ensuring that the rectification factor of the ionic diode is not hindered by high ionic strength buffers, which is difficult to achieve with nanofluidic diodes due to Debye screening.[26]

We can also control the threshold in the forward direction of the ionic diode by choosing different V_B values. The conductive side of the ionic diode shown in Fig. 2c demonstrates that the "on" threshold is roughly 4 V for $V_B = -20$ V, 6 V for $V_B = -30$ V and 10.5 V for $V_B = -40$ V. It is because a higher forward potential (a higher V_D) is needed to induce ion enrichment at the intersection region when a larger potential drop is applied in the "G-B" control fluidic channel (a lower V_B) to generate ion depletion.

A solid state transistor, such as a bipolar junction transistor (BJT) or a field-effect transistor (FET), can realize electron current switching using a control signal through the base terminal (BJT) or the gate terminal (FET) and electron current amplification from an input to an output. Current efforts on ionic transistors allow small ion current switching (nanoampere range);[6,7,12] however, independent amplification of the ion current is required. Here, by changing the electrical connection to the terminals, our device can be operated as an ionic transistor which can allow both large ion current switching and ion current amplification through the "D-S" output fluidic channel. As schematically shown in Fig. 3a, the "B" terminal and the "S" terminal are co-grounded to configure an ionic transistor. The applied voltage at the "G" terminal V_G serves as the control voltage to render the ionic transistor either an ion current switch or an ion current amplifier.

Fig. 3a illustrates the switching mechanism of the ionic transistor. Due to the high conductivity of the 0.1× PBS solution, the "D-S" output fluidic channel can conduct a high ion current even without a control voltage, indicating that the ionic transistor is usually at the "ON" state, as the ion concentration at the intersection region is not depleted. In addition, under a negative V_G (for example, −10 V), the ion concentration at the intersection region is enriched, giving rise to an even higher output current I_{output} for the "ON" state. The ion enrichment by the negative control voltage is sche-
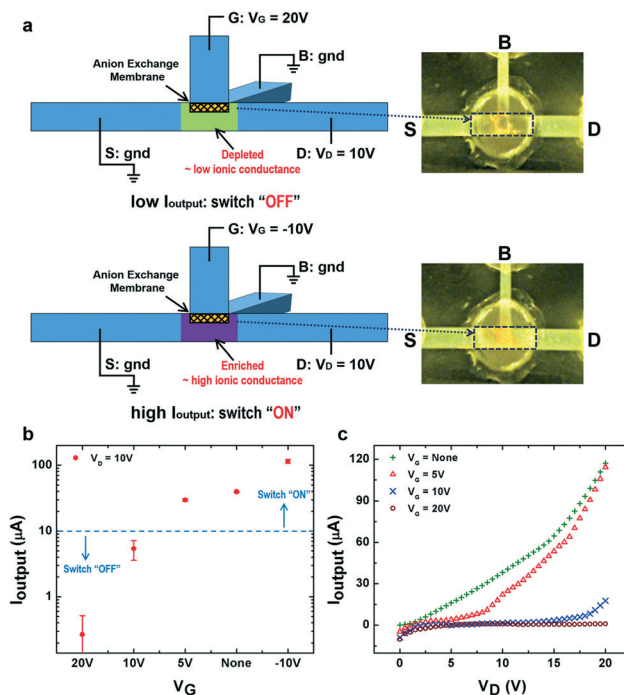

Fig. 3 (a) Schematics of the electrical operation method and the switching mechanism of the ionic transistor. The fluorescence images show the ion depletion at the "OFF" state (the upper panel) and the ion enrichment at the "ON" state (the lower panel) in the intersection region. (b) The output currents under different control voltage V_G values show the switching of the ionic transistor. I_{output} is measured for 10 min in each measurement. (c) The output I–V characteristics show the effective "switching-off" region for different V_G values of the ionic transistor. V_D is swept from 0 V to 20 V in each measurement.

matically shown in the lower panel of Fig. 3a, and verified by the high fluorescence intensity observed at the intersection region (the highlighted frame). To switch off the ionic transistor, as seen from the schematics in the upper panel of Fig. 3a, a positive control voltage V_G is applied (for example, 20 V). It generates an ion depletion zone at the intersection region to switch off I_{output} with a low conductance in the ion depletion zone that "*blocks*" the "D-S" output fluidic channel, as confirmed by the low fluorescence intensity at the intersection region (the highlighted frame on the right).

To show the switching operation of the ionic transistor, the output current is measured for 10 minutes when V_D is set at 10 V, under different control voltage (V_G) conditions (Fig. 3b). Without applying V_G, the I_{output} is 40 μA which is the intrinsic "ON" state current of the "D-S" output fluidic channel. When a negative V_G (−10 V) is applied, which induces ion enrichment at the intersection region, the "ON" state I_{output} is enhanced to 114 μA. In contrast, when a sufficiently positive V_G is applied to induce ion depletion, the "OFF" state I_{output} is below 10 μA, which is 5 μA for $V_G = 10$ V and 0.27 μA for $V_G = 20$ V. The on–off ratio of the ionic transistor can hence be as high as 422 between the "ON" and "OFF" state, and the "ON" state can deliver a current larger than 100 μA. Since a positive V_G with respect to ground is needed to generate the ion depletion zone, too high an

output voltage drop (positive V_D compared to gnd) may convert the local potential at the intersection region close to or higher than V_G, which undermines the ion depletion and results in loss of the "OFF" state. Fig. 3c shows the effective "switching-off" range at different V_G values. The I_{output} is measured at different V_D values from 0 V to 20 V under fixed positive control voltage values of V_G = 5 V, 10 V and 20 V. The I_{output} under no applied V_G shows the intrinsic "ON" state current. It can be seen that, for V_D values larger than 6 V when V_G = 5 V or for V_D values larger than 17 V at V_G = 10 V, the I_{output} starts to rise which means that the ionic transistor fails to be switched "OFF". Whereas for V_G = 20 V, the ionic transistor is successfully maintained at the "OFF" state for the entire range of output voltage drops. These data indicate that an appropriate control voltage V_G needs to be chosen for the specific output voltage difference of each application.

It is well known that a semiconductor field-effect transistor can amplify an input signal when it works in the "saturation mode", where a carrier depletion zone "pinches off" the conductive channel due to a decrease in the potential difference between the gate terminal and the drain terminal (which is similar to the potential at the "G" terminal and the "D" terminal in our fluidic device).[4] By changing the potential of our terminals and controlling the two competing fields, we show an analog "saturation mode" for our ionic transistor, which is similar to those observed in semiconductor field-effect transistors, indicating the capability of our device to amplify the ion current through the AEM to the output fluidic channel (the "D" terminal).

The amplification mechanism is shown in Fig. 4a and the I_{output}-V_D characteristics under different V_G inputs are shown in Fig. 4b. For our current experimental set-up with the AEM, a relatively low negative input voltage V_G (−1 V, −2.5 V, −5 V or −7 V) and a negative output voltage V_D are applied in measuring the I_{output}-V_D characteristics. Two distinct regions are observed: the amplification region and the linear region of the ionic transistor. When the absolute value of V_D is smaller than or comparable to the absolute value of the input V_G, the ion concentration at the intersection region remains at a high buffer value or is slightly enriched. This is because the potential above the AEM V_G is lower than the potential at both the grounded "S" and "B" terminals and the potential drop from "G" to "D" is either negative or not sufficiently positive to generate ion depletion underneath the membrane. Hence, the "D-S" output fluidic channel behaves like a linear conductive channel, resulting in a linear region, as shown in Fig. 4b. However, once the absolute value of V_D becomes high, for example, when V_D < −11 V at V_G = −1 V, the potential difference between V_G and V_D is high enough to render the local potential at the intersection region $V_{junction}$ sufficiently lower than V_G to generate depletion at the intersection region through the "G-D" channel instead of the "G-B" channel. This ion depletion zone "pinches off" the "D-S" output fluidic channel, giving rise to the limiting output current I_{output} which does not change with increasing $|V_D|$.[5,11] The ionic transistor therefore functions in the amplification re-
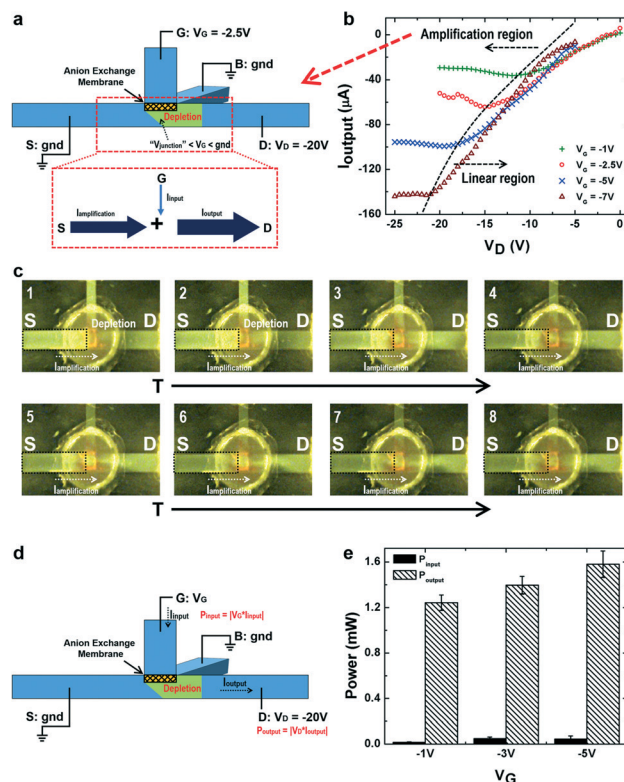

Fig. 4 (a) Schematics of the amplification mechanism of the ionic transistor. (b) The I_{output}-V_D characteristics under different V_G values show the linear region and the amplification region of the ionic transistor. V_D is swept from 0 V to −20 V for V_G = −1 V and −2.5 V, and from −5 V to −25 V for V_G = −5 V and −7 V. (c) Real-time fluorescence images show the current amplification from the "S" terminal adding to the output current. 1: t = 600 s; 2: t = 856 s; 3: t = 1519 s; 4: t = 1821 s; 5: t = 2077 s; 6: t = 2228 s; 7: t = 2349 s; 8: t = 2454 s. (d) Experiment set-up for measurement of the input and amplified output power. (e) The comparison between the input and output power shows the amplification and the output power control by the input potential V_G. The average power amplification factor is 45.

gion, as shown in Fig. 4b. Since $V_{junction}$ is even lower than the potential at the "S" terminal (gnd) when ion depletion occurs, an amplification current $I_{amplification}$ flows from the "S" terminal to the intersection region and is added onto the input current from the membrane I_{input}, thus resulting in an amplified output current I_{output} to the "D" terminal (Fig. 4a). A higher $|V_G|$ produces a lower $V_{junction}$ in the amplification region. Hence, a larger potential drop between the "S" terminal and the intersection region leads to a higher $|I_{amplification}|$, and consequentially, a larger amplified $|I_{output}|$. As shown in Fig. 4b, a V_G of −7 V can achieve a larger than 140 μA $|I_{output}|$. Fig. 4c verifies the amplification mechanism. V_G is set as −2.5 V, while V_D is −20 V. The ion depletion zone with low fluorescence intensity is developed from the intersection region to the "D" terminal 600 s after the start of the experiment, as seen from the 1 and 2 fluorescence images. As time evolves, the fluorescence intensity in the highlighted frame decreases as the positively charged fluorescent dye is transported from the "S" terminal side to the "D" terminal

side, demonstrating that $I_{\text{amplification}}$ is added to I_{output} to achieve amplification. The real-time fluorescence video showing the $I_{\text{amplification}}$ can be found in the ESI.† We characterize the amplification capability of this first prototype of our ionic transistor by comparing the input and output power (Fig. 4d). The input power is expressed as $P_{\text{input}} = |V_{\text{G}} \times I_{\text{input}}|$ and the output power is expressed as $P_{\text{output}} = |V_{\text{D}} \times I_{\text{output}}|$. We fix V_{D} at −20 V and measure the input and output power at V_{G} = −1 V, −3 V, and −5 V. The results in Fig. 4e show that the ionic transistor can deliver an output power of more than 1 mW, and achieve power amplification by a factor of 45. The output power is regulated by the input voltage V_{G}. This feature allows us to further proportionally amplify small ion currents or potential inputs to larger ion current outputs to acquire better signals or to drive downstream ion current circuits. Since the amplified output current is invariant with respect to output potential drops (V_{D}) in the amplification region, the ionic transistor can drive a wide range of ionic circuit loads in series or in parallel, thus enabling integrated ionic circuits.

The geometrical design of the microfluidic channel-AEM coupled chip (Fig. 1a) ensures the stable output of the ionic circuit platform for both diode and transistor operations. Since electroconvection vortices may grow from the membrane surface under a high DC electric field to diminish the depletion zone, we design the microfluidic channel plane to be parallel to the depletion side of the membrane with a small separation (250 μm). The resulting large hydrodynamic resistance has been shown to be very effective in suppressing the vortex instability.[27,28] Stable ion depletion or enrichment can hence be sustained along the microfluidic channel even under a relatively high applied voltage (e.g., 20 V). In addition, the output ion conductance of the output fluidic channel is only regulated by the ion concentration at the intersection region, and is not affected by the growth of the ion depletion and enrichment zones in the perpendicular "G-B" control fluidic channel outside the intersection region. Therefore, the output current and the diode/transistor functionalities remain stable once the ion concentration condition is established in the intersection region after around a hundred seconds. As a result of this geometrical design, the ionic circuit chip can operate at a high input voltage of up to 50 volts to meet the goal of high-flux operations. We choose a lower value of 25 volts as our upper limit to ensure that the buffer pH is not affected by electrolysis reactions at the electrodes. If the buffer pH is not an issue, stable operation at up to 50 volts is possible. The ionic circuit chip is also robust in complex electrolytes with different ions, because the AEM we choose, with 1 nm pores, has a high ion exchange capacity of 1.8 mval g^{-1} that remains stable at high ionic strengths and in the presence of multivalent ions (see the ESI†).[15] We intentionally use a complex high ionic-strength electrolyte system (PBS) containing various single and multi-valent ions to demonstrate the versatility of our chip. The same chip is tested repeatedly over four months with no obvious changes in functionalities, indicating the robustness of the design.

Conclusions

We report a high-flux multifunctional ionic circuit chip that can be used either as an ionic diode or an ionic transistor, depending on the electrical operation method. The ion current output of the device can exceed a hundred microamperes, which is two to three orders of magnitude higher than those of other reported ionic circuits. However, it offers a rectification factor of 176 for the ionic diode, an on–off ratio of 422 and a 45-fold power amplification for the ionic transistor in high ionic strength buffers (0.1× PBS). Since the output ionic flux is not restricted by the ion-selective medium (AEM), an arbitrary dynamic range can be designed with different channel dimensions to achieve scalability. These characteristics make our chip suitable as the basic element for integrated and scalable large-scale ionic circuits. The lithography-free fabrication process is amenable to low-cost polymer-based mass manufacturing processes. The relatively long response time of a few hundred seconds can be improved if we scale down the channel dimension to tens of microns, with a corresponding trade-off in current flux. However, for most biomedical applications, a response time of a few minutes is more than adequate. Hence, we believe that the chip can lead to a new ionic circuit platform for a variety of applications.

Acknowledgements

References

1　H. Chun and T. D. Chung, *Annu. Rev. Anal. Chem.*, 2015, **8**, 441.

2　H.-J. Koo and O. D. Velev, *Biomicrofluidics*, 2013, 7, 031501.

3　W. Guan, S. X. Li and M. A. Reed, *Nanotechnology*, 2014, **25**, 122001.

4　S. M. Sze and K. K. Ng, *Physics of semiconductor devices*, John Wiley & Sons, 2006.

5　G. Yossifon, P. Mushenheim, Y.-C. Chang and H.-C. Chang, *Phys. Rev. E: Stat., Nonlinear, Soft Matter Phys.*, 2009, **79**, 046305.

6　R. Karnik, R. Fan, M. Yue, D. Li, P. Yang and A. Majumdar, *Nano Lett.*, 2005, **5**, 943.

7　R. Karnik, K. Castelino and A. Majumdar, *Appl. Phys. Lett.*, 2006, **88**, 123114.

8　E. B. Kalman, I. Vlassiouk and Z. S. Siwy, *Adv. Mater.*, 2008, **20**, 293.

9　H.-J. Koo, S. T. Chang and O. D. Velev, *Small*, 2010, **6**, 1393.

10　H. Daiguji, J. Hwang, A. Takahashi, S. Kataoka and A. Endo, *Langmuir*, 2012, **28**, 3671.

11　Z. Slouka, S. Senapati and H.-C. Chang, *Annu. Rev. Anal. Chem.*, 2014, 7, 317.

12　K. Tybrandt, K. C. Larsson, A. Richter-Dahlfors and M. Berggren, *Proc. Natl. Acad. Sci. U. S. A.*, 2010, **107**, 9929.

13 L.-J. Cheng and H.-C. Chang, *Biomicrofluidics*, 2011, **5**, 046502.

14 E. O. Gabrielsson, K. Tybrandt and M. Berggren, *Lab Chip*, 2012, **12**, 2507.

15 S. Senapati, Z. Slouka, S. S. Shah, S. K. Behura, Z. Shi, M. S. Stack, D. W. Severson and H.-C. Chang, *Biosens. Bioelectron.*, 2014, **60**, 92.

16 D. Taller, K. Richards, Z. Slouka, S. Senapati, R. Hill, D. B. Go and H.-C. Chang, *Lab Chip*, 2015, **15**, 1656.

17 K. Tybrandt, R. Forchheimer and M. Berggren, *Nat. Commun.*, 2012, **3**, 871.

18 K. C. Larsson, P. Kjäll and A. Richter-Dahlfors, *Biochim. Biophys. Acta*, 2013, **1830**, 4334.

19 H.-J. Koo, J.-H. So, M. D. Dickey and O. D. Velev, *Adv. Mater.*, 2011, **23**, 3559.

20 G. Sun, Z. Slouka and H.-C. Chang, *Small*, 2015, **11**, 5206.

21 L.-J. Cheng and H.-C. Chang, *Lab Chip*, 2014, **14**, 979.

22 E. Choi, K. Kwon, D. Kim and J. Park, *Lab Chip*, 2015, **15**, 168.

23 D. K. Kim, C. Duan, Y. F. Chen and A. Majumdar, *Microfluid. Nanofluid.*, 2010, **9**, 1215.

24 U. Vermesh, J. W. Choi, O. Vermesh, R. Fan, J. Nagarah and J. R. Heath, *Nano Lett.*, 2009, **9**, 1315.

25 Z. Slouka, S. Senapati, S. Shah, R. Lawler, Z. Shi, M. S. Stack and H.-C. Chang, *Talanta*, 2015, **145**, 35.

26 Y. Yan, L. Wang, J. Xue and H.-C. Chang, *J. Chem. Phys.*, 2013, **138**, 044706.

27 H.-C. Chang, G. Yossifon and E. A. Demekhin, *Annu. Rev. Fluid Mech.*, 2012, **44**, 401.

28 G. Yossifon, P. Mushenheim and H.-C. Chang, *Europhys. Lett.*, 2010, **90**, 64004.